QUARTERLY JOURNAL OF THE ROYAL METEOROLOGICAL SOCIETY

Q. J. R. Meteorol. Soc. **00**: 1–11 (2009)

Published online in Wiley InterScience

(www.interscience.wiley.com) DOI: 10.1002/qj.000

Three-dimensional evolution of ensemble forecast spread during the onset of a stratospheric sudden warming event in January 2006

Kazuaki NISHII*, Hisashi NAKAMURA

Department of Earth and Planetary Science, Graduate School of Science, University of Tokyo, Japan.

Abstract: A set of simple sensitivity analyses applied to a set of operational ensemble forecasts reveals that prediction skill of a stratospheric sudden warming event observed in late January 2006 is particularly sensitive to uncertainties in the initial state in the vicinity of a developing synoptic-scale cyclone observed over the North Pacific more than two weeks prior to the peak of the event. For the first few days in the forecast, the local maximum of the forecast spread is translated eastward in association with observed downstream development of synoptic-scale disturbances that was initiated from the Pacific cyclone. The spread then reaches into the subpolar North Atlantic, where a blocking ridge acted as the source of an upward-propagating Rossby wave packet that gave rise to the deceleration of the stratospheric polar-night jet (PNJ). Following the observed wave packet, the maximum forecast spread is translated upward from the ridge and finally reaches into the stratosphere, causing a large forecast spread in the PNJ deceleration.

KEY WORDS Rossby wave packet, downstream development, blocking, initial error

Received ; Revised ; Accepted

1 Introduction

During a stratospheric sudden warming (SSW) event, the stratospheric polar vortex warms up by several tens of degrees. The polar-night jet (PNJ) concomitantly weakens and, in prominent events, turns into easterly within a few days. It is now accepted that an SSW event, regarded as manifestations of the negative phase of the stratospheric Northern Annular Mode (NAM), tend to turn the tropospheric NAM into the negative phase subsequently (Baldwin and Dunkerton, 1999, 2001; Limpasuvan *et al.*, 2004). Thus misforecast of an SSW event may lower the skill for an extended forecast of the extratropical troposphere. Actually, Charlton *et al.* (2004, 2005) have shown through their ensemble forecast experiments that initial stratospheric conditions modified by artificially-induced initial errors can influence the tropospheric condition after SSW events.

A series of studies on predictability of SSW events

*Correspondence to: Department of Earth and Planetary Science, Graduate School of Science, University of Tokyo, Tokyo, 113-0033, Japan. E-mail: nishii@eps.s.u-tokyo.ac.jp

has recently been conducted by using operational ensemble forecasts produced by the Japan Meteorological Agency (JMA). Mukougawa and Hirooka (2004), for example, have revealed that the amplification of tropospheric planetary waves was essential for an SSW event observed in the 1998/99 winter. Mukougawa *et al.* (2005) have pointed out through another forecast experiment that, in addition to changes in the zonal-mean westerlies around the tropopause, the formation of a blocking ridge over Europe was an important factor for the enhancement of upward propagation of planetary-wave activity into the stratosphere during an SSW event in December 2001. Hirooka *et al.* (2007) have found a tendency that a major SSW event to which the zonal wavenumber one component contributes dominantly with no preceding minor events shows higher predictability than a major SSW event to which the higher wavenumber components mainly contribute with one or more preceding minor SSW events.

A major SSW event was observed in January 2006 (Manney *et al.*, 2008). Prior to this event, the zonal-mean PNJ had gradually weakened from late December 2005 associated with several events of enhanced upward propagation of planetary wave activity from the troposphere. Nishii *et al.* (2009; hereafter NNM09) have found that those events were contributed to significantly by zonally-confined Rossby wave packets propagating into the stratosphere from tropospheric quasi-stationary circulation anomalies. In one of these events that occurred just before the PNJ turning into easterly in mid-January, a Rossby wave packet that emanated from a tropospheric anticyclonic circulation anomaly over the North Atlantic was found to be the primary contributor to the enhanced upward injection of planetary-wave activity. The tropospheric anticyclonic anomaly was amplified by vorticity flux divergence associated with synoptic-scale transient eddies along the Atlantic storm track whose intensification was due to their downstream development from the North Pacific.

Figure 1(a) shows time series of 20-hPa zonal-mean zonal wind velocity for the individual ensemble forecast members operated by the JMA with their initial conditions taken from the observations on 11 or 12 January 2006 (red, blue and green lines without any symbols). The spread of the predicted wind velocity among the members increases rapidly with time in the period between 21 and 28 January, during which the observed 20-hPa PNJ (a black line with open squares) underwent the most rapid deceleration in the SSW event. Concomitantly, a large spread is also observed in the meridional eddy heat flux at the 100-hPa level (Figure 1(b)), which is a measure of the injection of planetary wave activity from the troposphere into the stratosphere that causes deceleration of the PNJ. Many of the members can predict the amplification of the flux until around 17 January, though. While the observed heat flux continued to exceed 20 K m s^{-1} for the next several days, most of the ensemble members apparently underestimate the flux especially after 20 January, which might cause the misforecast of the PNJ deceleration after 21 January.

The aim of this study is to analyze the growth of initial errors among the ensemble members, which finally induced the large ensemble spread in the PNJ prediction for the particular SSW event. By tracing the three-dimensional evolution of the ensemble spread and conducting a singular vector analysis and a simple sensitivity analysis for the ensemble members, we show that the large ensemble spread of the predicted intensity of the 20-hPa PNJ during the SSW event (Figure 1(a)) arises largely

DOI: 10.1002/qj

from the ensemble spread of the predicted upward emanation of a Rossby wave packet from a tropospheric anticyclonic anomaly over the Atlantic. We also show that the prediction skill of the anticyclonic anomaly is sensitive to the initial errors around a synoptic-scale cyclone developing upstream over the North Pacific, observed about two weeks before the peak of the SSW event.

2 Data

The ensemble forecast product utilized in this study was produced by the JMA Operational Monthly Forecast System (JMA 2002), where initial perturbation fields were constructed by a combination of the Breeding of Growing Modes (BGM) method (Toth and Kalnay 1993) and the Lagged Average Forecasting (LAF) method (Hoffman and Kalnay, 1983). We use a particular set of the JMA forecasts with their initial fields taken for 11 or 12 January 2006. For each of the initial dates six different (”positive”) perturbation fields were generated by the BGM method. The ensemble members were doubled by including the same perturbation fields but with their polarity reversed (”negative”). With the unperturbed initial field included, the total number of the ensemble members is thus 13 for each of the initial dates.

The spread among the ensemble members is regarded as a measure of uncertainty in the ensemble forecast. The spread is defined at each grid point as the local variance of a particular variable among the ensemble members about its ensemble mean. Observational fields for the verification have been provided by the JMA Climate Data Assimilation System (JCDAS), as a continuation from the Japanese 25-year Reanalysis (JRA-25; Onogi *et al.*, 2007). The ensemble prediction system operated around the period of the SSW event used the same forecast model as in the JRA-25 assimilation system, which is reported to have a cold bias in the lower and middle stratosphere (Onogi *et al.*, 2007). While the cold bias in the assimilation system does not emerge in the JRA-25 data as long as observational data are available in the stratosphere, the ensemble forecasts may suffer from it in a significant manner.

3 Three dimensional evolution of the forecast spread

Figure 2 indicates the distributions of the local ensemble spread in the lower stratosphere with shading for the selected days as indicated. Because its magnitude increases with time, the spread for a given forecast day has been normalized by its instantaneous maximum within the domain (poleward of 20°). Contours are for observed geopotential-height anomalies that are defined as local deviations from the climatology. On 16 January, just before the initiation of the rapid PNJ deceleration (Figure 1(a)), the large spread is confined to the subpolar North Atlantic (Figure 2(a)). The maximum ensemble spread is almost stationary throughout the rapid PNJ deceleration from 20 to 28 January (Figures 2(b) and 2(c)).

As shown in Figure 3, the ensemble spread over the North Atlantic undergoes upward extension from the troposphere into the stratosphere. On 16 January (Figure 3(a)), the spread is confined to the vicinity of a tropospheric anticyclonic anomaly around 40°W associated with a prominent blocking flow configuration (Figure 4(b)). It acted as the source of a Rossby wave packet that propagated into the stratosphere (NNM09). In fact, the stratospheric cyclonic anomaly over western Europe amplified as the tropospheric anticyclonic anomaly weakened (Figures 3(a) and 3(b)) and phase lines of the height anomalies were tilting westward with height (Figure 3(a)). These features indicate group velocity propagation of a

DOI: 10.1002/qj

Rossby wave packet over the North Atlantic. Interestingly, unlike in the troposphere, the ensemble spread in the stratosphere is not maximized near the centre of the cyclonic anomaly. Rather, it is maximized around its node line adjacent to the tropospheric anticyclonic anomaly on 18 January (Figure 3(b)) and then 2 days later around another node line adjacent to a stratospheric anticyclonic anomaly (Figure 3(c)). Furthermore, the cyclonic anomaly centres of the individual ensemble members over Europe, denoted by black dots in Figures 2(a) and 2(b), become more scattered as the forecast spread extends upward into the stratosphere. We thus conjecture that the forecast spread extends into the stratosphere in association with the Rossby wave packet that contributed to the SSW event, probably reflecting differences in its magnitude, group velocity and/or wavelengths simulated among the ensemble members. The upward extension of the forecast spread into the stratosphere starts around 16 January, when most of the ensemble members fail to predict the persistent wave-activity propagation into the stratosphere (Figure 1(b)).

NNM09 pointed out that the tropospheric anticyclonic anomaly over the subpolar North Atlantic (Figure 4(b)), from which the ensemble spread extends into the stratosphere (Figure 3), developed by 16 January in association with downstream development of synoptic-scale disturbances from the North Pacific into the North Atlantic. In fact, observed maxima of the squared 250-hPa meridional wind velocity apparently show a signature of group velocity propagation across the region from 11 to 16 January (Figure 5(a)). Crude estimations of the group velocity (rectangle with solid line) and phase speed (dashed line) based on Figure 5(a) are about 30° and 10° in longitude per day, respectively. The former appears to correspond to the zonal group velocity of baroclinic wave packet (Chang 1993), while the latter is in agreement with typical zonal phase speed of synoptic-scale baroclinic waves (Wallace *et al.* 1988). Correspondingly, the local maximum of ensemble forecast spread of 250-hPa meridional wind velocity appears to translate zonally across the Northeastern Pacific slowly (about 6° per day), while the downstream extension of local maxima of the forecast spread is also hinted, as indicated by a rectangle with a solid line in Figure 5(b). The propagation speed of the spread maxima into the Atlantic is about 25° in longitude per day, which is similar to but slightly slower than the group velocity of the observed wave packet in Figure 5(a). Eastward translation of forecast errors across the North American continent associated with downstream development has been reported by Langland *et al.* (2002). In the case they analyzed, the eastward propagation of the errors was faster than the phase speed of synoptic-scale troughs and ridges and slightly slower than a wave packet propagation. These features are also found in our analysis. Our analysis is also consistent with the result of Rabier *et al.* (1996), who showed that forecast errors propagate downstream from the North Pacific or North America as far as into Europe by comparing forecasts started from routinely constructed analyses with those from initial values improved by the adjoint method.

On 12 January, one of the initial days for the ensemble forecasts we analyzed, local maxima of the ensemble spread in the 250-hPa geopotential height are found not only over the North Pacific but also over North Africa and South Asia (Figure 4(a)). However, the growth of the latter two spread maxima is less than that of the North Pacific maximum located just downstream of the particular cyclone that appears to be the origin of the "downstream development" of the ensemble spread. The corresponding spread maximum is also observed in SLP over

DOI: 10.1002/qj

the North Pacific around the particular surface cyclone (not shown).

4 Cluster analysis among the ensemble members

The "group-velocity" propagation of the forecast spread shown in the preceding subsection (Figure 5(b)) may represent inconsistency among the ensemble members in phase and/or amplitude of eddy components developing downstream. To confirm this, a cluster analysis based on the Ward's method was applied to 250-hPa geopotential height predicted by the ensemble members for 14 January over the Pacific (Figure 1(c)). Through the analysis, the members have been categorized into three clusters. The particular number of the clusters has been determined subjectively after several trials.

Two of the three clusters identified are found to be well defined, one (Cluster A) characterized by relatively fast phase speed and small eddy amplitudes (red contours in Figure 1(c)), and the other (Cluster B) by slower phase speed and larger eddy amplitudes (blue contours). The third cluster (green contour), which consists only of a single member, is an outlier and therefore not discussed below. It is noteworthy that in Cluster A, the blocking high over the North Atlantic, which is regarded as the source for the upward-propagating wave packet (Figures 3 and 4(b)), tends to develop more strongly with more pronounced poleward meanders of the westerlies than in Cluster B and in the observations as well (Figure 1(d)). This feature is particularly obvious in 2 members of Cluster A for which the PNJ deceleration is successfully predicted (red thick line in Figure 1(a)) and the tropospheric westerlies exhibit pronounced poleward meanders over the Atlantic (red thick contour in Figure 1(d)). The two members predicted the upward wave-activity flux to be stronger than in the observations (Figure 1(b)), but the predicted PNJ deceleration is nevertheless comparable to the observations (Figure 1(a)). Forecast members that predict realistic PNJ deceleration tend to overestimate the blocking intensity. This suggests that unrealistically strong upward flux of planetary wave activity may be necessary in the forecast model for decelerating the PNJ as much as in the real atmosphere associated with the SSW event, which might be due to the cold bias in the forecast model (Onogi *et al.* 2007). These results imply that the mechanisms of planetary wave amplification into the stratosphere in individual ensemble members may not necessarily be the same as in the real atmosphere, as long as the forecast model has a non-negligible bias.

5 SVD analysis

Singular value decomposition (SVD) analysis was applied to all the 26 ensemble forecast members, in order to confirm the relationship between the development of the Atlantic anticyclonic anomaly (Figure 4(b)) and initial errors as well as other forecasted fields. The SVD analysis is often applied to time-varying fields of two variables to extract their dominant co-variability based on their temporal covariance matrix (Bretherton *et al.* 1992). In our application, SVD is applied to a cross covariance matrix whose element is the covariance between deviations of a given variable among the 26 members from its local ensemble mean at a given grid point for a particular forecast time and the corresponding deviations of any variable at any grid point for any forecast time. In each of our applications, each field has been normalized by its standard deviation among the ensemble members, and the matrix is therefore a cross-correlation matrix rather than a covariance matrix. We focus on the leading SVD mode that has the largest singular value and therefore explains

DOI: 10.1002/qj

the largest fraction (more than 40% in our applications) of their spatially-integrated squared covariance.

A set of SVD analysis was performed between the ensemble of 250-hPa geopotential height field forecasted for 16 January over the North Atlantic (270°E-357.5°E, 40°N-85°N), where the blocking was observed, and the same or other forecast ensemble over the entire extratropical northern hemisphere (northward of 30°N). Each panel of Figure 6 shows a hemispheric map of the heterogeneous regression coefficient of a given variable for a particular forecast time with the normalized expansion coefficients of the first SVD mode for the 26 members of the 250-hPa height over the North Atlantic forecasted for 16 January. In each of the panels, we can therefore identify regions where forecast spread at a given forecast time is particularly sensitive to the spread of the blocking high signature in the 250-hPa height over the subpolar North Atlantic forecasted for 16 January. The corresponding heterogeneous regression map of 250-hPa height forecasted over the North Atlantic for 16 January with the expansion coefficients among the members of the particular variable and forecast time is similar to the pattern shown in Figure 6(c), which represents uncertainties in the intensity of the blocking.

Figure 6(a) indicates that the large forecast spread in 250-hPa height over the North Atlantic for 16 January is most sensitive to uncertainties in the initial field of 250-hPa height confined into two regions over the North Pacific on 12 January. Specifically, a positive signal in Figure 6(a) is located slightly upstream of a positive 250-hPa height anomaly observed on 12 January near the date line (Figure 4(a)) and downstream of the cyclonic anomaly that has been identical as the origin of the downstream development of synoptic disturbances (Figure 5(a)). The corresponding maximum sensitivity in the 1000-hPa geopotential height field on 12 January is observed over the central North Pacific (Figure 6(d)). Again, this positive signal is located slightly upstream of a surface pressure ridge developing downstream of the surface cyclone (Figures 7(b) and (d)).

The SVD results indicate that the amplification of the North Atlantic blocking ridge in the forecast for 16 January is sensitive to the synoptic circulation over the North Pacific in the initial state. More specifically, the positive height signal just upstream of the ridge suggests that a synoptic wave packet that consist of the pressure ridge and trough over the North Pacific tends to be shorter (longer) in zonal wave length for the ensemble members with stronger (weaker) development of the North Atlantic blocking. The wave packet with shorter wave length tends to accompany stronger meridional wind velocity fluctuations and thus stronger zonal component of wave-activity flux than that with longer wave length, yielding stronger downstream development across the Pacific and North America that can lead to enhanced development of the Atlantic blocking.

The same SVD analysis as above but for the hemispheric field of 250-hPa height forecasted for 14 January reveals the significant negative correlation between forecasted strength of the North Atlantic ridge for 16 January and geopotential height forecasted for 14 January around the east coast of North America (Figure 6(b)). A comparison with Figure 1(c) indicates that this negative correlation is a manifestation of the sensitivity of the blocking ridge development to the intensity of the cyclonic anomaly upstream that constitutes the wave packet developing toward downstream.

The SVD analysis with the forecasted 250-hPa height over the subpolar North Atlantic is also applied to the

DOI: 10.1002/qj

spread of the upward flux of local Rossby wave activity (Takaya and Nakamura 2001) evaluated at the 100-hPa level for the individual forecast members for 18 January (Figure 6(e)). The analysis indicates that the wave-activity flux locally into the stratosphere from the tropospheric anticyclonic anomaly over the North Atlantic tends to increase with the amplitude of the anomaly (Figure 6(e)). This result is in agreement with the tendency observed in Figure 1 that the stronger meander of the tropospheric westerlies over the North Atlantic is more favorable for the stronger upward wave propagation into the stratosphere. Our SVD analysis further demonstrates that large forecast spread in 50-hPa height over the North Atlantic for 20 January (Figure 2) is most sensitive to the amplitude of the tropospheric blocking ridge forecasted underneath a few days earlier (Figure 6(f)), in a manner consistent with the magnitude of the upward wave-activity flux (Figure 6(e)). The strongest sensitivity and maximum forecast spread in 50-hPa height forecasted for 20 January are identified around the node of the circulation anomalies actually observed (Figure 2(b)), suggesting that scattered cyclonic anomaly centres among the ensemble members for 20 January (Figure 2(b)) may arise from the forecast errors in the strength of the tropospheric blocking ridge over the North Atlantic.

6 Simple sensitivity analysis

Finally, we have conducted a simple sensitivity analysis introduced by Enomoto *et al.* (2006, 2007) to reconfirm the aforementioned results. The simple sensitivity analysis utilizes a result of an ensemble forecast to identify initial perturbations that can grow optimally during a given forecast period in a given verification region. We firstly give a brief explanation on the analysis following Enomoto *et al.* (2006).

Suppose that time evolution of the i-th ensemble member ($i = 1, 2, \cdots, m$) may be expressed as

$$\mathbf{z}_i = M\mathbf{y}_i, \tag{1}$$

where $\mathbf{y}_i$ and $\mathbf{z}_i$ are initial and forecasted perturbations, respectively, and M denotes a mapping operator. Note that the perturbations here are defined as deviations from the unperturbed member but not from the ensemble average. With matrices Y and Z that consist of $\mathbf{y}_i$ and $\mathbf{z}_i$ as their columns, respectively, linear combinations of initial and forecasted perturbations can be expressed as

$$\mathbf{y} = p_1\mathbf{y}_1 + p_2\mathbf{y}_2 + \cdots + p_m\mathbf{y}_m = Y\mathbf{p} \tag{2}$$

and

$$\mathbf{z} = p_1\mathbf{z}_1 + p_2\mathbf{z}_2 + \cdots + p_m\mathbf{z}_m = Z\mathbf{p} \tag{3}$$

respectively, with a vector $\mathbf{p}$ that consists of the coefficients p_i. Then one can find a particular $\mathbf{p}$ that maximizes the norm of $\mathbf{z}$ ($\|\mathbf{z}\|$) in the verification region under the constraint that the norm of $\mathbf{y}$ ($\|\mathbf{y}\|$) equals to unity. Here, $\|\mathbf{y}\|^2$ and $\|\mathbf{z}\|^2$ are defined as

$$\|\mathbf{y}\|^2 = <\mathbf{y}^T, G\mathbf{y}> = \mathbf{p}^T Y^T G Y \mathbf{p}, \tag{4}$$

and

$$\|\mathbf{z}\|^2 = <\mathbf{z}^T, H\mathbf{z}> = \mathbf{p}^T Z^T H Z \mathbf{p}. \tag{5}$$

In our application, the norm of an arbitrary perturbation $\mathbf{x}$ is defined in terms of dry total energy as

$$\begin{aligned} \|\mathbf{x}\|^2 &= <\mathbf{x}^T, F\mathbf{x}> \\ &= \frac{1}{2}\iint_A \{u'^2 + v'^2 \\ &\quad + \frac{C_p}{T_r}T'^2 + RT_r(\frac{p'_s}{p_r})^2\} dA dp, \end{aligned} \tag{6}$$

DOI: 10.1002/qj

where u', v', T' and p'_s denote perturbations in the zonal and meridional wind velocities, temperature and surface pressure. In Equation (6), C_p and R denote the specific heat at constant pressure and the gas constant, respectively of dry air, T_r and p_r signify the reference value of temperature, and pressure, respectively at the surface, A denotes the specified horizontal domain for analysis, and F is the operator that symbolically defines the particular energy norm over the given domain. In our analysis, the operator matrix G in Equation (4) was chosen in such a manner that the dry total energy of the initial perturbations was integrated horizontally over the northern hemisphere poleward of 30° N and vertically from the 1000- to 100-hPa levels for each of the initial dates of the forecast (11 or 12 January). Likewise, the operator H was determined to express the dry total energy of the forecast field over a given verification domain, as specified below.

To find $\mathbf{p}$ that maximizes $\|\mathbf{z}\|^2$, the Lagrange multiplier method is used for finding the extrema of f,

$$f(\mathbf{y}, \lambda) = \mathbf{p}^T Z^T H Z \mathbf{p} - \lambda(\mathbf{p}^T Y^T G Y \mathbf{p} - 1), \quad (7)$$

by differentiating f with respect to $\mathbf{p}$, keeping in mind that H and G are symmetric, as

$$\frac{\partial f(\mathbf{y}, \lambda)}{\partial \mathbf{p}} = 2(Z^T H Z \mathbf{p} - \lambda Y^T G Y \mathbf{p}) = \mathbf{0}. \quad (8)$$

This leads to a generalized eigenvalue problem

$$Z^T H Z \mathbf{p} = \lambda Y^T G Y \mathbf{p}. \quad (9)$$

By substituting $\mathbf{p}$ obtained by solving Equation (9) into Equation (2), we can estimate initial perturbations that will evolve into the most developed perturbation over the given forecast within the verification domain. We used only the first eigenvector for each of our analysis as discussed below, whose eigenvalue accounts for nearly 40% of the sum of all the eigenvalues. Thus one may infer that domains with particularly large initial perturbations in terms of the dry total energy (Equation (6) but without horizontal integration) are the most sensitive domains for the forecast within the given verification domain.

Ideally, the analysis requires a large numbers of independently perturbed forecast members. As noted in section 2, however, only six members have been independently perturbed out of the 12 perturbed members for each of the initial dates in the JMA ensemble forecast we utilize. Still, there are totally 64 ($= 2^6$) combinations that can be formed for our sensitivity analysis by assigning the polarity (either "positive" or "negative") of the six independently perturbed members. For each of the 64 combinations, we evaluated the vertically-integrated total energy (based on Equation (6) without horizontal integration) locally for solving Equation (9) for the first eigenvector before taking its are average.

For the first exercise of our sensitivity analysis, the verification time and domain were set to be 16 January and a region over the subpolar North Atlantic (310°E-340°E and 50°N-65°N), respectively, where the forecast spread was maximized around the developing blocking anticyclone (Figure 4b). The matrix H in Equation (5) was determined so that the dry total energy was integrated horizontally over the subpolar North Atlantic and vertically from the 1000- to 100-hPa levels. As shown in Figures 7(a) and 7(b), the sensitivity to the initial state for either 11 or 12 January measured as the tropospheric dry total energy is found to be maximized locally around surface cyclones migrating eastward over the North Pacific. This result is in agreement with our findings based on the SVD analysis.

The same analysis was repeated but with the matrix

DOI: 10.1002/qj

H in Equation (5) determined for the entire stratospheric polar and subpolar domain (100- to 10-hPa levels and poleward of 50°N) on 28 January, when the PNJ was most weakened (Figure 1(a)). Even for the forecast period longer than two weeks (15 to 16 days in this case), the maximum of sensitivity in the initial state is found again over the North Pacific. Particularly, the upstream component of the cyclone pair exhibits higher sensitivity. In fact, our analysis in section 3 has suggested that the surface cyclone, which developed rapidly while moving northeastward from (165°E, 40°N) to (170°E, 46°E) from 11 to 12 January, acted as the origin of the downstream development of the ensemble spread. Thus initial observational errors around the particular developing cyclone over the Pacific are again shown to be one of the factors that induce large discrepancies in the SSW prediction among the ensemble members. The maximum sensitivity over the Northwestern Pacific is consistent with Buizza and Palmer (1995), who showed that the Northwestern Pacific is one of the most dynamically unstable areas as indicated by singular vectors.

7 Development of the ALERA-analyzed spread

The AFES-LETKF [†] experimental ensemble reanalysis (ALERA; Miyoshi and Yamane, 2007; Miyoshi *et al.*, 2007) provides us with initial perturbation fields and associated spread among ensemble members based on time-evolving flow fields [‡], which gives us uncertainties in the particular reanalysis. On 11 and 12 January, the ALERA-based initial spread over the North Pacific is maximized in the vicinity of the particular developing cyclone discussed above (Figure 8). This result suggests that large uncertainties in the intensity and/or the central position of the cyclone added some difficulties to the particular SSW forecast.

The ALERA-based spread maxima show their eastward development across the North Pacific as far as 120°W with speed of about 12° in longitude a day (Figure 5(c)), following the migration of the particular low-pressure system. This relatively slow development of the spread can also be seen in the JMA ensemble forecast spread (Figure 5(b)). Uncertainties in observations and the corresponding ALERA-analyzed spread both tend to be reduced over the North American continent, where more observations are available than over the Pacific. Since ALERA does not assimilate satellite-based observations, observational data available for ALERA are relatively few over the oceans. In ALERA, the propagation of spread maxima that corresponds to the group velocity of the observed wave packet (Figure 5(a)) is not quite obvious, which may also be due to the larger number of observations available for ALERA over the North American continent.

From a hemispheric viewpoint, the ALERA-based spread in the troposphere was maximized around the prominent anticyclonic anomaly observed over the subpolar North Atlantic (not shown), in agreement with the JMA forecast ensemble spread maximum for 16 January (Figure 4(b)). In the stratosphere, ALERA-based spread around 16 January was also maximized over the North Atlantic (not shown), where the forecast ensemble spread was growing on that day (Figures 2(a) and 2(b)).

8 Concluding remarks

By using a product of the JMA monthly ensemble forecast system, we have analyzed the time evolution of the forecast spread among the ensemble members before a major SSW event observed in late January 2006. As the source

[†] AFES is the abbreviation for the AGCM for the Earth Simulator, and LETKF for Local Ensemble Transform Kalman Filter.
[‡] ALERA is available via OPenDAP (http://www3.es.jamstec.go.jp/).

DOI: 10.1002/qj

of the ensemble forecast spread (i.e., uncertainties in the forecast) for the SSW event, we have identified errors in the initial state in the vicinity of a synoptic-scale cyclone developing over the North Pacific about two weeks before the SSW event. In growing with time, the initial errors are then translated as forecast errors eastward into a blocking ridge over the subpolar Atlantic for the following few days and then upward into the stratosphere to cause the large ensemble forecast spread in the PNJ deceleration. The propagation of the forecast errors is associated with downstream development of synoptic-scale disturbances in the troposphere and followed by upward propagation of a Rossby wave packet, both of which have been found to be important dynamical processes for the occurrence of the particular SSW event (NNM09). We have found the time evolution of the forecast spread consistent with the result of our sensitivity analysis, which shows that the predictions of the SSW event and its precursory formation of the tropospheric blocking anomaly over the North Atlantic both tend to be particularly sensitive to local errors in the vicinity of a particular cyclone developing over the North Pacific in the initial field for the forecast. We have confirmed these results through our SVD analysis for the JMA ensemble forecast and our analysis of the ALERA-analyzed spread whose development is similar to the JMA forecast spread.

At the time of January 2006, a set of ensemble forecast was conducted in the JMA monthly forecast system only once a week with the limited number of independent ensemble members. Furthermore, the forecast model at that time is known to suffer from a cold bias in the stratosphere. Thus more frequent ensemble forecasts with a larger ensemble size based on a less biased forecast model are needed to confirm our findings in the present study. We are planning to conduct a set of ensemble hindcast integrations for the SSW event we analyzed with initial fields taken from the ALERA system. Recently, Mukougawa and Hirooka (2007) have suggested that improvement in SSW prediction does not necessarily yield better extended forecast of the tropospheric circulation. Mukougawa *et al.* (2009) have showed that prediction skill of the tropospheric NAM is better when the stratospheric NAM is negative. Since those studies are, however, based only on a particular SSW event or those only over five winters, more SSW events must be analyzed to assess their influence on the predictability of the tropospheric circulation system.

Acknowledgements

The authors are particularly grateful to Dr. T. Enomoto for his useful advices not only on the sensitivity analysis but also on ALERA data. Discussion with Dr. Y. J. Orsolini was invaluable. The ensemble forecast data used in this study were provided by way of the ”Meteorological Research Consortium”, a framework for research cooperation between the JMA and Meteorological Society of Japan. The JRA-25 dataset is provided by the JMA and the Central Research Institute of Electric Power Industry (CRIEPI). This study is supported in part by the Japanese Ministry of Education, Culture, Sports, Science and Technology under the Grant-in-Aid for Scientific Research (A) #18204044. The Grid Analysis and Display System (GrADS) was used for drawing the figures.

References

Baldwin MP, Dunkerton TJ. 1999. Propagation of the Arctic Oscillation from the stratosphere to the troposphere. *J. Geophys. Res.*, **104:** 30937–30946.

Baldwin MP, Dunkerton TJ. 2001. Stratospheric harbingers of anomalous weather regimes. *Science*,**294** 581–584.

DOI: 10.1002/qj

Bretherton CS, Smith C, Wallace JM. 1992 An intercomparison of methods for finding coupled patterns in climate data sets. *J. Climate*, **5:** 541–560.

Buizza R, Palmer TN. 1995. The singular-vector structure of the Atmospheric global circulation. *J. Atmos. Sci.*, **52:** 1434–1456.

Chang EKM. 1993. Downstream development of baroclinic waves as inferred from regression analysis. *J. Atmos. Sci.*, **50:** 2038–2053.

Charlton AJ, O'Neill A, Lahoz WA, Massacand AC, Berrisford P. 2004 Sensitivity of tropospheric forecasts to stratospheric initial conditions. *Q. J. R. Meteorol. Soc.*, **130:** 1771–1792.

Charlton AJ, O'Neill A, Lahoz WA, Massacand AC, Berrisford P. 2005 The impact of the stratosphere on the troposphere during the southern hemisphere stratospheric sudden warming, September 2002. *Q. J. R. Meteorol. Soc.*, **131:** 2171–2188.

Enomoto T, Yamane S, Ohfuchi W. 2006. Simple sensitivity analysis using ensemble forecast. *Proceedings of 3rd workshop on mechanisms of climate variation and its predictability*, 40–43. (In Japanese).

Enomoto T, Ohfuchi W, Nakamura H, Shapiro MA. 2007. Remote effects of tropical storm Cristobal upon a cut-off cyclone over Europe in August 2002. *Meteorol. Atmos. Phys.*, **96**, 29–42.

Hirooka T, Ichimaru T, Mukougawa H. 2007. Predictability of stratospheric Sudden warmings as inferred from ensemble forecast data: Intercomparison of 2001/02 and 2003/04 winters. *J. Meteorol. Soc. Jpn.*, **85:** 919–925.

Hoffmann RN, Kalnay E. 1983. Lagged average forecasting, an alternative to Monte Carlo forecasting. *Tellus*, **35A**, 100-118.

Japan Meteorological Agency. 2002. Outline of the operational numerical weather prediction at the Japan Meteorological Agency. Appendix to WMO Numerical Weather Prediction Progress Report, Tokyo, 158 pp.

Kalnay E. 2003. Atmospheric modeling, data assimilation and predictability. Cambridge University Press, pp341.

Langland RH, Shapiro MA, Gelaro R. 2002. Initial condition sensitivity and error growth in forecasts of the 25 January 2000 east coast snowstorm. *Mon. Weather Rev.*, **130:** 957–974.

Limpasuvan V, Thompson DWJ, Hartmann DL. 2004. The life cycle of the Northern Hemisphere sudden warmings. *J. Climate*, **17:** 2584–2596.

Manney GL, Krüger K, Pawson S, Minschwaner K, Schwartz MJ, Daffer WH, Livesey NJ, Mlynczak MG, Remsberg EE, Russell III JM, Waters JW. 2008. The evolution of the stratopause during the 2006 major warming: Satellite data and assimilated meteorological analyses. *J. Geophys. Res.*, **113**, D11115, doi:10.1029/2007JD009097.

Miyoshi T, Yamane S. 2007. Local ensemble transform Kalman filtering with an AGCM at a T159/L48 resolution. *Mon. Weather Rev.*, **135:** 3841–3861.

Miyoshi T, Yamane S, Enomoto T. 2007. The AFES-LETKF experimental ensemble reanalysis: ALERA. *SOLA*, 3, 45-48.

Mukougawa H, Hirooka T. 2004. Predictability of stratospheric sudden warming: A case study for 1998/99 winter. *Mon. Weather Rev.*, **132:** 1764–1776.

Mukougawa H, Sakai H, Hirooka T. 2005. High sensitivity to the initial condition for the prediction of sudden warming. *Geophys. Res. Lett.*, **32**, L17806, doi:10.1029/2005GL022909.

Mukougawa H, Hirooka T. 2008. Predictability of the downward migration of the Northern Annular Mode: A case study for January 2003. *J. Meteorol. Soc. Jpn.*, **85:** 861–870.

Mukougawa H, Hirooka T, Kuroda Y. 2009. Influence of stratospheric circulation on the predictability of the tropospheric Northern Annular Mode. *Geophys. Res. Lett.*, **36**, doi:10.1029/2008GL037127

Nishii K, Nakamura H. Miyasaka T. 2009. Modulations in the planetary wave field induced by upward-propagating Rossby wave packets prior to stratospheric sudden warming events: A case study *Q. J. R. Meteorol. Soc.*, **135:** 39–52

Onogi K, Tsutsui J, Koide H, Sakamoto M, Kobayashi S, Hatsushika H, Matsumoto T, Yamazaki N, Kamahori H, Takahashi K, Kadokura S, Wada K, Kato K, Oyama R, Ose T, Mannoji N, Taira R. 2007. The JRA-25 Reanalysis. *J. Meteorol. Soc. Jpn.*, **85:** 369–432.

Rabier F, Klinker E, Hollingsworth A. 1996. Sensitivity of forecast errors to initial conditions. *Q. J. R. Meteorol. Soc.*, **122:** 121–150.

Takaya K, Nakamura H. 2001. A formulation of a phase-independent wave-activity flux for stationary and migratory quasi-geostrophic eddies on a zonally basic flow. *J. Atmos. Sci.*, **58:** 608–627.

Toth Z, Kalnay E. 1993. Ensemble forecasting at NMC; the generation of perturbations. *Bull. Amer. Meteor. Soc.*,**74**, 2317-2330.

Wallace JM, Lim GH, Blackmon ML. 1988. Relationship between cyclone tracks, anticyclone tracks and baroclinic wave-guides. *J. Atmos. Sci.*, **45:** 439–462.

DOI: 10.1002/qj

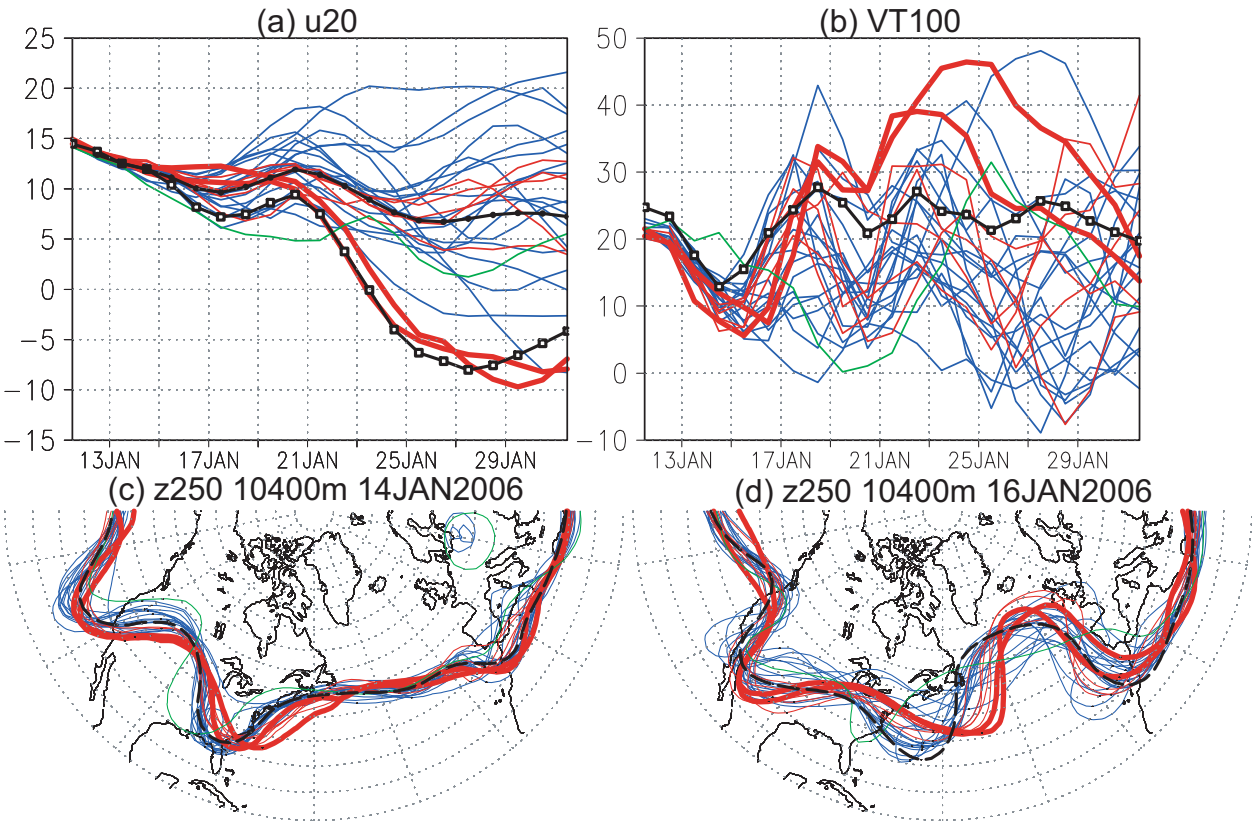

Figure 1. (a) Time series of 20-hPa zonal-mean zonal wind (ms^{-1}) averaged over 50°N-80°N. Lines without any symbols denote the individual ensemble members starting on either 11 or 12 January 2006. Lines with closed circles and with open squares denote the ensemble average and observation based on the reanalysis data, respectively. (b) The same as in (a), but for zonal-mean 100-hPa eddy heat flux averaged over 50°N-80°N, where eddy components of meridional wind velocity and temperature are defined as deviations from their zonal-mean components. (c) 10400-m isolines of 250-hPa geopotenital height for individual ensemble members predicted for 14 January and the corresponding observation (dashed black line). (d) The same as in (c) but for 16 January. In each panel, blue, red and green lines indicates the ensemble members grouped into three by a cluster analysis based on 250-hPa geopotenital height on 14 January over the region (180°-300°E, 20°N-60°N) as shown in (c). The clusters indicated by blue, red and green lines include 18, 7 and 1 members, respectively. Two thick lines in each panel are for the members that apparently succeeded in the prediction of PNJ deceleration.

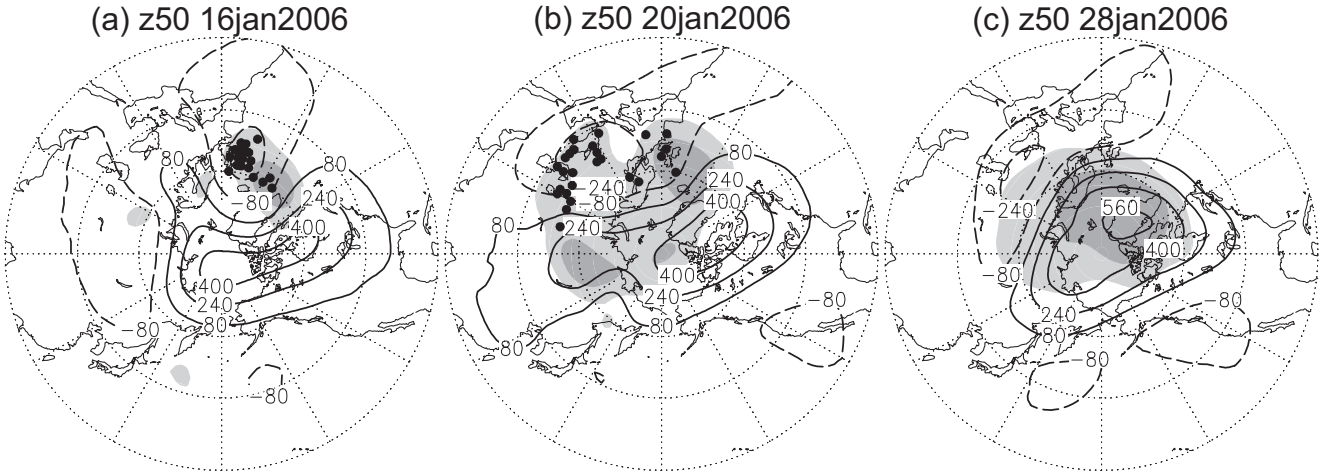

Figure 2. (a) Local spread of 50-hPa geopotential height predicted for 16 January 2006 (shaded for lightly and heavily for 0.3 - 0.6 and values greater than 0.6, respectively), superimposed on observed 50-hPa height anomalies contoured for ($\pm$ 80, $\pm$ 240, $\pm$ 400, $\pm$ 560 m; dashed for negative values). The spread has been normalized by its instantaneous maximum within the domain poleward of 20°N. (b) As in (a) but for 20 January 2006. (c) As in (a) but for 28 January 2006. In (a) and (b), black dots indicate the centers of 50-hPa cyclonic anomalies over Europe predicted in the individual ensemble members.

Prepared using qjrms3.cls
DOI: 10.1002/qj

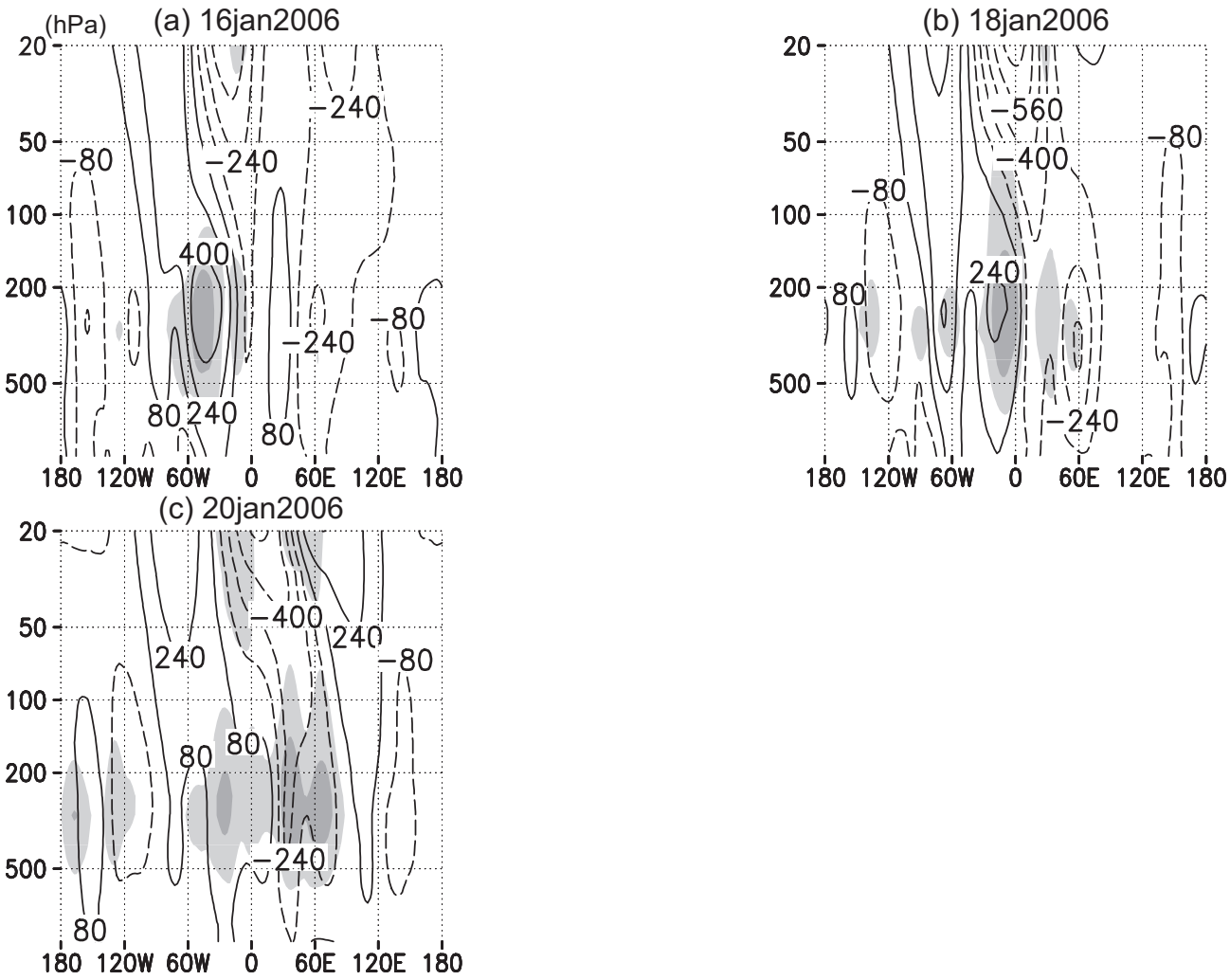

Figure 3. (a) A zonal cross section for 50°N of the local spread of forecasted geopotential height predicted for 16 January 2006, with shading lightly and heavily for 0.3 - 0.6 and values greater than 0.6, respectively. The spread has been normalized by its maximum value over the particular domain shown above. Superimposed with contours are geopotential height anomalies as local departures from the climatology ($\pm$ 80, $\pm$ 240, $\pm$ 400, $\pm$ 560 m; dashed for negative). (b) As in (a) but for 18 January 2006. (c) As in (a) but for 20 January 2006.

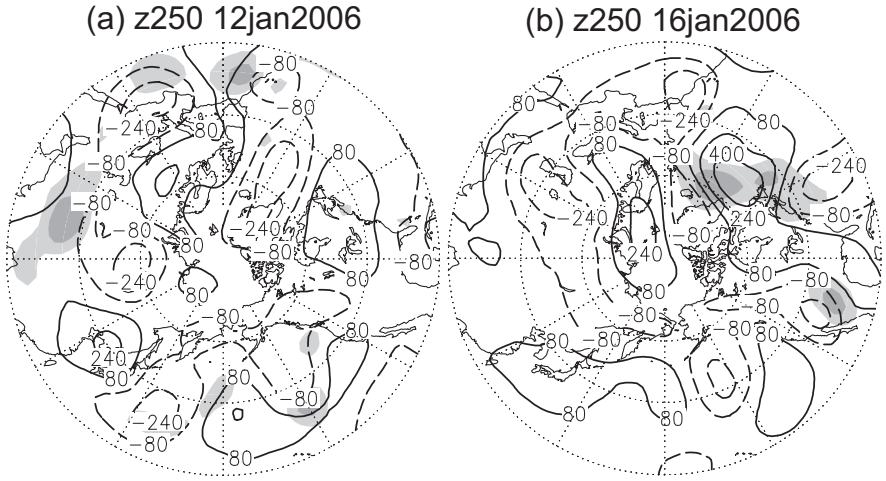

Figure 4. As in Figure 2(a), but for 250-hPa height for (a) 12 and (b) 16 January 2006.

DOI: 10.1002/qj

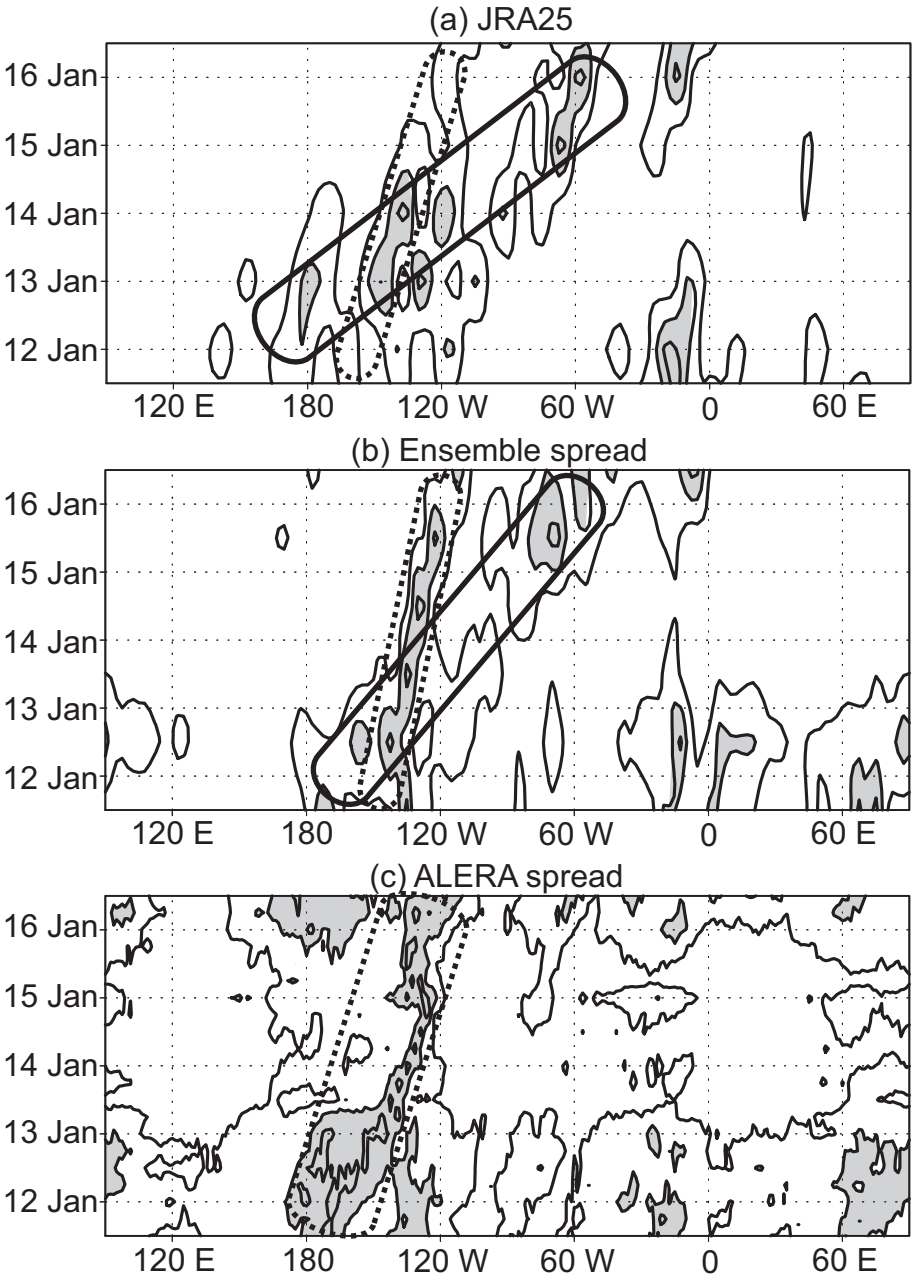

Figure 5. (a) A Hovmöller diagram of the squared meridional wind velocity (v) observed at 250-hPa level averaged between 20° and 60°N, which has been normalized by its maximum for each day over the longitudinal span as indicated (shaded for the quantity over 0.6). (b) As in (a) but for the spread in predicted 250-hPa v among the forecast ensemble members with the initial date of 11 January. Note that the corresponding plot with the members from 12 January gives qualitatively the same picture. (c) As in (a) but for the spread in 250-hPa v among the members of ALERA. In each panel, solid and dashed rectangles are plotted for crude estimations of group velocity and phase speed, respectively.

DOI: 10.1002/qj

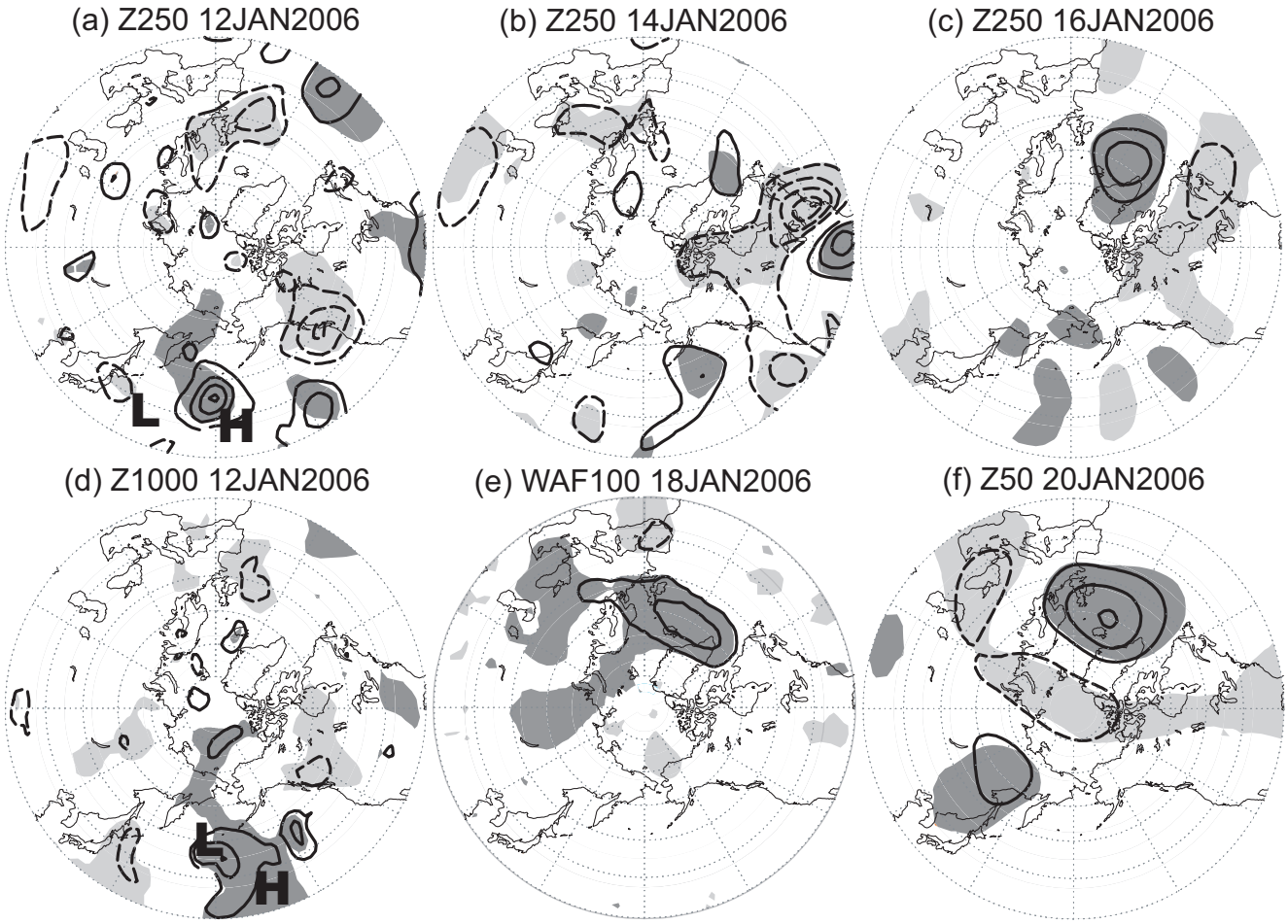

Figure 6. Results of SVD analysis based on the JMA ensemble forecast applied to the spread of 250-hPa height over the subpolar North Atlantic forecasted for 16 January 2006 with the forecast spread of (a-c) hemispheric 250-hPa height (a) for 12 January (contour interval is 10 m), (b) for 14 January (contour interval is 20 m), and (c) for 16 January (contour interval is 100 m). Dashed contours are for negative. Heavy and light shading denotes the correlation exceeds 0.4 and falls bellow -0.4, respectively. (d-f) As in (a-c), but with the spread of (d) 1000-hPa height on 12 January, (contour interval is 10 m), (e) 100-hPa upward wave-activity flux on 18 January (contour interval is 0.01 $m^2\ s^{-2}$) and (f) 50-hPa height on 20 January (contour interval is 50 m). Panels (a-f) show heterogeneous regression maps of the given value all with the normalized expansion coefficient of 250-hPa geopotential height over the Atlantic, which represent typical deviations from the ensemble mean state in forecast members that predict the strong North Atlantic blocking than the ensemble mean. The labels H and L in (a) denote anticyclonic and cyclonic anomalies observed on 12 January (Figure 4(a)), while the labels H and L in (d) denote a ridge and cyclone, respectively, observed at the surface on 12 January (Figure 7(b)).

DOI: 10.1002/qj

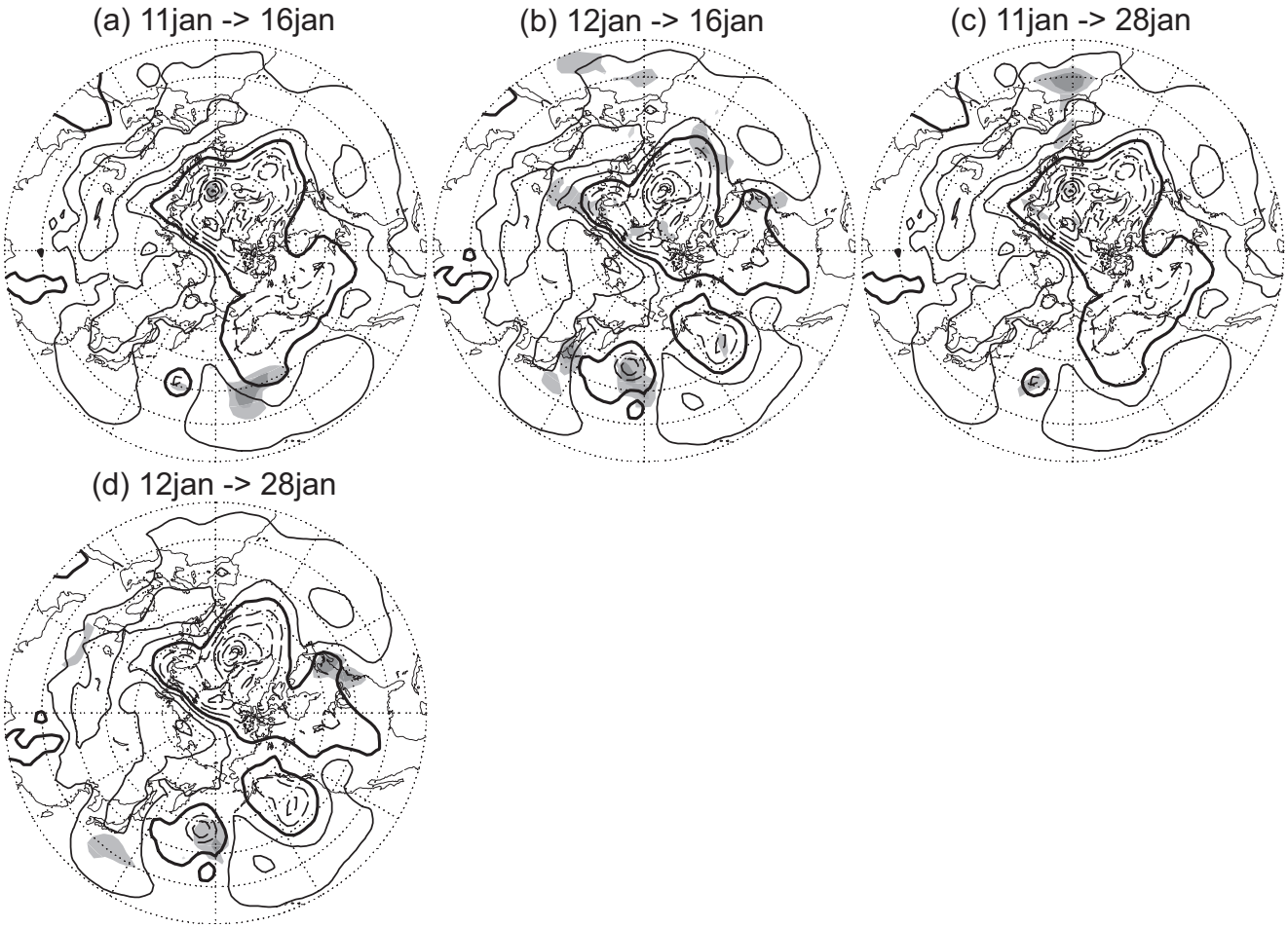

Figure 7. Results of a sensitivity analysis based on the JMA ensemble forecast. (a) Areas of the high sensitivity in the initial tropospheric field to the forecasted intensity of a tropospheric North Atlantic blocking ridge presented as total energy averaged between 1000- and 250-hPa levels, normalized by a maximum value within the domain poleward of 20°N (Shaded lightly and heavily for 0.3 - 0.6 and values greater than 0.6, respectively). The verification domain is between 310°E and 340°E, 50°N and 65°N, 1000- and 250-hPa level on 16 January 2006 with ensemble members starting on 11 January 2006. Contours are for sea level pressure of JRA-25 (every 10 hPa; Dashed for less then 1010 hPa; Thick solid contours for 1010 hPa). (b) Same as in (a) but with ensemble members starting on 12 January 2006. (c) Same as in (a) but for the sensitivity in the initial tropospheric field on 11 January 2006 to the forecasted lower stratospheric (100-50hPa) field over the entire domain poleward of 50°N for 28 January 2006. (d) Same as in (a) but for the initial field on 12 January 2006.

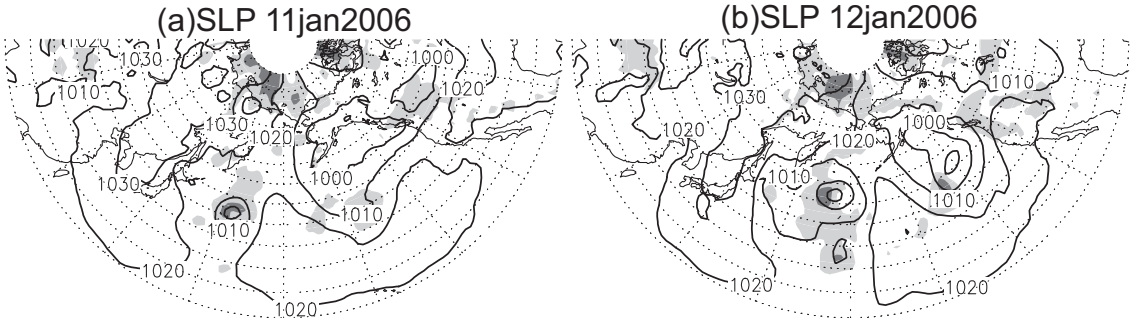

Figure 8. (a) Sea level pressure on 11 January 2006 produced by ALERA (contoured for every 10 hPa). Shaded lightly and heavily where the ensemble spread is between 1 and 2 [hPa] and greater than 2 [hPa], respectively. (b) As in (a) but for 12 January.

DOI: 10.1002/qj